Vehicle System Dynamics
Vol. 47, No. 6, June 2009, 701–720

Taylor & Francis
Taylor & Francis Group

Stability measurement of high-speed vehicles

Steven C. Peters* and Karl Iagnemma

Department of Mechanical Engineering, Massachusetts Institute of Technology, Cambridge, MA, USA

(*Received 13 September 2007; final version received 13 July 2008*)

Vehicle rollover represents a significant percentage of single-vehicle accidents and accounts for over 9000 fatalities and over 200,000 non-fatal injuries each year. Previous research has yielded rollover stability control systems that are effective in on-road conditions. Accident statistics show, however, that over 90% of rollovers involve road departure, during which a vehicle may encounter sloped and rough terrain while travelling at high speed. A critical element of most rollover stability control systems is a metric that monitors a vehicle's nearness to rollover. Most metrics, however, are designed for use on flat, level surfaces characteristic of on-road terrain. In this paper, a new stability metric, termed the stability moment, is proposed that is accurate on terrain surfaces with arbitrary geometry, which allows it to be used in road departure scenarios. The metric is based on an estimate of the distribution of wheel–terrain contact forces. The metric can be calculated on line in real time, using only practical, low-cost sensors. The metric is compared in simulations and experimental studies to existing stability metrics and is shown to exhibit superior performance, particularly in off-road conditions.

Keywords: rollover stability; contact force distribution; road departure; ADAMS modelling; measurement

1. Introduction

A significant amount of research and development effort over the past 40 years has been devoted to improving the safety of passenger vehicles. Despite these efforts, in the United States in 2004 more than 40,000 people were killed and 2.5 million injured in motor vehicle accidents, at an estimated economic cost of $200 billion. Of these accidents, rollover is particularly fatal, accounting for more than 9000 deaths and 200,000 injuries. Rollovers constituted just 2.3% of total accidents but over 10% of fatal accidents, and trailed only head-on collisions and collisions with pedestrians in this unfortunate ratio [1]. Studies have shown that over 80% of passenger vehicle rollovers involve road departure [2]. Road departure is a critical destabilising event, since off-road features such as terrain slope, roughness, and deformability can substantially degrade vehicle stability [3].

Rollover is also a significant threat to high-speed mobile robots, which have recently been the focus of substantial research activity, highlighted by the interest in DARPA's Grand Challenge autonomous vehicle race [4]. Applications of high-speed robots include exploration,

*Corresponding author. Email: scpeters@mit.edu

ISSN 0042-3114 print/ISSN 1744-5159 online

DOI: 10.1080/00423110802344636
http://www.informaworld.com

reconnaissance, and material delivery. These systems are designed to operate on natural terrain that may be sloped, slippery, rough, and deformable. Unfortunately, these systems are susceptible to rollover, particularly while performing severe manoeuvres. Despite the fact that many systems are designed with rugged chassis (and some are designed to be mechanically invertible), rollover accidents often disable the robot and/or damage its payload. Rollover accidents have been reported in the literature [5] and have been experienced by the authors during field experiments.

A variety of yaw stability and roll stability control systems designed for on-road scenarios have been proposed in the literature [6–8] and implemented in production passenger vehicles [9]. A critical element of most rollover stability control systems is a metric that monitors a vehicle's nearness to rollover. Most metrics, however, are designed for use on flat, level surfaces characteristic of on-road terrain. This paper presents a technique for rollover stability measurement that additionally applies to sloped and rough surfaces characteristic of off-road terrain. The proposed metric is intended to for use as feedback in the next generation of off-road rollover stability control systems.

2. Literature review

Most existing work in rollover stability measurement can be grouped into three categories: those based on geometric stability measures, energy-based stability measures, and contact force stability measures.

A number of metrics based on geometric principles have been developed for stability measurement. Researchers in mobile robotics have recognised that the location of the vehicle centre of gravity (c.g.) relative to the wheel–terrain contact points is critical to vehicle stability. The stability polygon (or support pattern) is defined as the convex hull of the polygon formed by wheel–terrain contact points projected onto a horizontal plane [10]. An early geometric measure defined stable vehicle configurations as those where the horizontal projection of the vehicle c.g. lies within this polygon [11]. A stability margin was then defined based on the shortest distance from the projected c.g. to a side of the polygon. Improvements to this measure were proposed [12,13]. However, this metric ignores the effects of changes in c.g. height and the destabilising influence of vehicle dynamic effects. It should be noted that a common geometric stability metric used in vehicle design is the static stability factor, which is computed as the ratio of vehicle width to c.g. height [14].

Another geometric measure, termed the force-angle stability measure, explicitly considers the effect of both internal and external forces acting on the vehicle [15], including gravity, inertial forces, and aerodynamic drag. The resultant of all forces (other than those due to wheel–terrain contact) is expressed at the vehicle c.g. If the line of action of the resultant force lies within the vehicle stability polygon, as illustrated in Figure 1a, the vehicle is considered stable. If the line of action lies outside the stability polygon, as in Figure 1b, the robot is considered

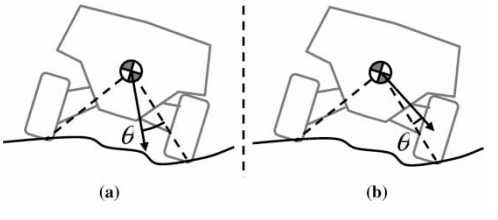

Figure 1. Illustration of force-angle measure [15]: (a) stable case, and (b) unstable case.

unstable, as a sustained application of forces along that line of action would eventually lead to rollover. The force-angle stability measure has been applied to low-speed articulating robots in a rough terrain [16], to a high-speed forklift on a flat floor [17], and to a high-speed mobile robot in rough terrain [18].

A second class of stability measures is based on estimates of stored vehicle energy. A tipover point is defined as the point where the vehicle c.g. lies directly above the line connecting an adjacent wheel pair. In this configuration, the vehicle possesses the maximum achievable potential energy (assuming at least two wheels remain in contact with the ground) and is semi-stable. The energy stability margin [19] measures the difference in potential energy between a vehicle's current state and its semi-stable state at tipover. This is a quasi-static method that has been applied to vehicles operating on rough terrain surfaces, though only at low speeds [19]. Dynamic energy-based stability measures have been proposed that analyse the difference between the vehicle's roll kinetic energy and potential energy. These measures have been applied to vehicles operating on flat ground at high speed [20,21].

A third class of stability measures is based on the distribution of wheel–terrain contact forces, and indicates nearness to wheel lift-off. Wheel lift-off is important as it is a necessary condition for rollover and can lead to reduced controllability. The load transfer metric, a common expression of contact force distribution, is defined by the difference in normal forces on the left and right side of a vehicle [6,7], as illustrated in Figure 2 and computed with Equation (1).

$$R = \frac{F_{\mathrm{R}} - F_{\mathrm{L}}}{F_{\mathrm{R}} + F_{\mathrm{L}}} \tag{1}$$

A practical implementation challenge associated with load transfer metrics is measuring wheel–terrain interaction forces, since direct measurement via wheel-mounted force transducers is impractical in most situations due to the high cost of these sensors. Force estimation based on measurement of suspension configuration (or state) can be used instead of direct force measurement [22–24], though this requires knowledge of suspension design parameters, which may be uncertain and time varying. Techniques for direct estimation of load transfer on flat ground with measurement of lateral acceleration [25,26], roll angle [7], or both [6] have been proposed that require minimal knowledge of suspension design parameters, though none of these methods have been evaluated in off-road scenarios.

This paper presents a method for measuring vehicle stability in off-road scenarios via a new metric termed the stability moment (SM). This metric can be considered a load transfer metric [15] and builds on previous work by the authors [18]. This metric estimates terrain contact forces from vehicle inertial quantities that can be measured with practical, low-cost sensors.

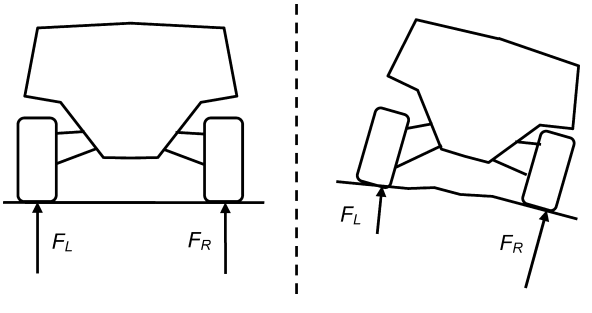

Figure 2. Force components in load transfer metric for flat terrain (left) and uneven terrain (right).

The method is validated with simulation and experimental results, and its performance is compared with existing techniques for stability measurement. A discussion of sensing requirements for measurement of the SM is also presented.

3. SM derivation

In this section, a model of a vehicle travelling on general uneven terrain is presented. This model will be used in the derivation of the SM metric.

3.1. *Vehicle model and direct SM definition*

A general l-wheeled vehicle is modelled as a multibody system of $l+1$ rigid bodies, representing the wheels and chassis. The inertial properties of the bodies are specified by mass m_i, inertia matrix $\mathbf{I}_i$, and c.g. position $\mathbf{c}_o^i$, $i \in \{1, \ldots, l+1\}$. Note that the vectors $\mathbf{c}_o$ are defined with respect to inertial frame {XYZ} at point O, and inertia matrices $\mathbf{I}_i$ are defined with respect to body fixed frames with associated rotation matrix $\mathbf{R}_o^i$ such that $\mathbf{I}_o^i = \mathbf{R}_o^i \mathbf{I}_i$. The angular velocity of each reference frame is given by $\boldsymbol{\omega}_i$ in its own coordinates and $\boldsymbol{\omega}_o^i$ in frame O. An illustration of this model for a four-wheeled vehicle is given in Figure 3. For clarity, two identical views are provided with different illustrated vectors.

In this multibody model, the wheels move and spin relative to the chassis, but all reaction forces between the chassis and wheels (i.e. suspension forces, powertrain torque, etc.) are internal to the system. This reduces the number of variables required to analyse the model. A caveat is that some dynamics of possible interest, such as those arising from sprung mass flexibility, shifting cargo, or sloshing fuel cannot be explicitly considered.

Each of the vehicle's l wheels may be in contact with an arbitrary terrain profile (i.e. flat, sloped, rough, etc.). It is assumed that the wheels make contact with the terrain at a single point. The wheel–terrain contact points are given by $\mathbf{p}_o^i$ and the corresponding contact forces by $\mathbf{F}_o^i$, $i \in \{1, \ldots, l\}$. The wheels are numbered in a counterclockwise manner when viewed from above, as shown in Figure 3. When a wheel is not in contact with the terrain (e.g. due to wheel hop), its contact point is placed at a point on the wheel where contact typically occurs.

It is assumed that the gravitational force $m\mathbf{g}$ acts at the c.g. of each body and that k other external forces $\mathbf{B}_o^i$ can act at points $\boldsymbol{q}_o^i$, $i \in \{1, \ldots, k\}$ on the vehicle. These forces can include aerodynamic drag, or collisions with other bodies.

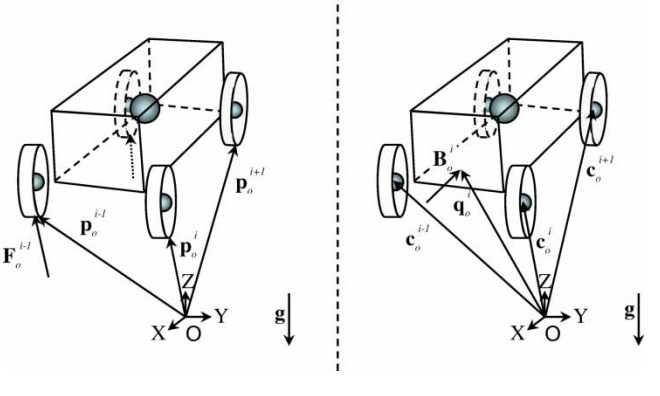

Figure 3. Vehicle model with four wheels.

Tipover axes, $\mathbf{r}_o^i$, are the lines connecting adjacent wheel–terrain contact points and represent the axes about which the vehicle pivots during rollover [15]. They are illustrated in Figure 4 and computed as:

$$\mathbf{r}_o^i = \frac{\mathbf{p}_o^{i+1} - \mathbf{p}_o^i}{\|\mathbf{p}_o^{i+1} - \mathbf{p}_o^i\|}, \quad i \in \{1, \ldots, l-1\} \tag{2}$$

$$\mathbf{r}_o^l = \frac{\mathbf{p}_o^1 - \mathbf{p}_o^l}{\|\mathbf{p}_o^1 - \mathbf{p}_o^l\|}, \quad i = l \tag{3}$$

A wheel–terrain contact force causes a moment about every tipover axis that does not pass through the forces' line of action. The magnitude of this moment is here employed as a basis for the proposed vehicle stability metric, termed the SM. The SM is computed with Equation (4), where $\mathbf{b}_o$ is any point on the tipover axis.

$$\mathrm{SM}_j = \left[\sum_{i=1}^{l} (\mathbf{p}_o^i - \mathbf{b}_o) \times \mathbf{F}_o^i \right] \cdot \mathbf{r}_o^j \tag{4}$$

Note that the vectors in Equation (4) are expressed in the inertial frame O. To compute SM in an arbitrary frame with rotation matrix $\mathbf{R}_b^o$, the vectors in Equation (4) are simply multiplied by $\mathbf{R}_b^o$:

$$\mathrm{SM}_j = \left[\sum_{i=1}^{l} \mathbf{p}_b^i \times \mathbf{F}_b^i \right] \cdot \mathbf{r}_b^j \tag{5}$$

with $\mathbf{p}_b^i \equiv \mathbf{R}_b^o(\mathbf{p}_o^i - \mathbf{b}_o)$, $\mathbf{F}_b^i \equiv \mathbf{R}_b^o \mathbf{F}^i{}_o$, and $\mathbf{r}_b^j \equiv \mathbf{R}_b^o \mathbf{r}_o^j$.

The SM is a measure of the destabilising influence of components of the wheel–terrain contact forces acting on the vehicle. This is illustrated in the example shown in Figure 5. Here, contact forces act on the left and right wheels, and are decomposed into components normal to the terrain surface (denoted N) and tangential to the surface (denoted T). Components of N and T parallel to the line connecting contact points do not affect the SM. Components perpendicular to the line connecting the contact points, denoted F_{L} and F_{R}, are the force components that do affect the SM.

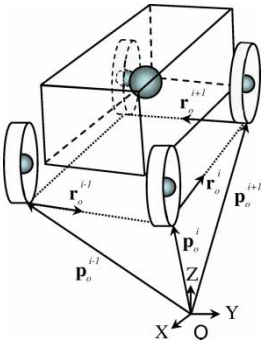

Figure 4. Tipover axes.

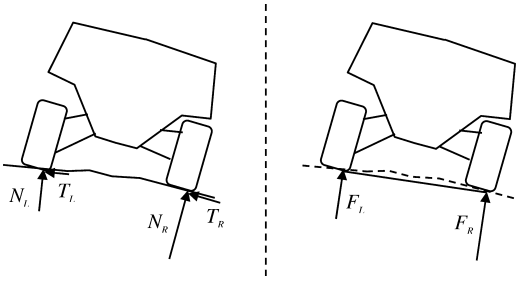

Figure 5. Components of terrain contact forces.

Since most passenger vehicles are much more susceptible to rollover about the left and right tipover axes (compared with the front and rear axes), a simplified value R_{SM} is defined as:

$$R_{\mathrm{SM}} = \frac{\mathrm{SM_L} - \mathrm{SM_R}}{\mathrm{SM_L} + \mathrm{SM_R}} \tag{6}$$

The nominal operating range of the metric, defined by the condition when all wheels are in contact with the ground, is given by the following:

$$-1 < R_{\mathrm{SM}} < 1 \tag{7}$$

It should be noted that during ballistic motion, when all wheels are off the ground, no contact forces act on the vehicle. Consequently all $\mathrm{SM}_j = 0$, which makes the quantity R_{SM} in Equations (6) and (7) undefined. An alternative to Equation (7) that is not undefined when all wheels are off the ground is:

$$-(\mathrm{SM_L} + \mathrm{SM_R}) < \mathrm{SM_L} - \mathrm{SM_R} < \mathrm{SM_L} + \mathrm{SM_R} \tag{8}$$

Though Equation (8) is a more well-posed stability condition, (6) and (7) are used for the remainder of this paper to facilitate comparison with other stability metrics.

3.2. *Indirect SM calculation*

In principle, the wheel–terrain contact forces required for calculation of the SM can be measured with wheel-mounted force sensors. As noted above, however, these sensors are costly and are not commonly present on passenger vehicles. To avoid this difficulty, an alternative expression for the SM is derived here. This expression is composed of inertial quantities that can be measured with practical, low-cost sensors. To avoid confusion in the remainder of this paper, the form of the SM defined in Equations (4) and (5) will be referred to as the direct form, and the alternative expression defined below will be referred to as the indirect form.

The indirect form of the SM is derived from angular momentum principles. Choosing the fixed point O as reference, conservation of angular momentum can be expressed as:

$$\mathbf{M}_o = \dot{\mathbf{H}}_o \tag{9}$$

where $\mathbf{M}_o$ is the sum of moments about point O caused by external forces acting on the vehicle, and is given by:

$$\mathbf{M}_o = \sum_{i=1}^{l} \mathbf{p}_o^i \times \mathbf{F}_o^i + \sum_{i=1}^{l+1} \mathbf{c}_o^i \times m_i \mathbf{g}_o + \sum_{i=1}^{k} \mathbf{q}_o^i \times \mathbf{B}_o^i \tag{10}$$

The term $\dot{\mathbf{H}}_o$ represents the change in angular momentum of the vehicle about point O. The angular momentum is given as:

$$\mathbf{H}_o = \sum_{i=1}^{l+1} (\mathbf{R}_o^i \mathbf{I}_i \boldsymbol{\omega}_i + \mathbf{c}_o^i \times m_i \dot{\mathbf{c}}_o^i) \tag{11}$$

Noting that $\dot{\mathbf{R}}_o^i = \boldsymbol{\omega}_o^i \times \mathbf{R}_o^i$, the time derivative of angular momentum is:

$$\dot{\mathbf{H}}_o = \sum_{i=1}^{l+1} (\boldsymbol{\omega}_o^i \times \mathbf{R}_o^i \mathbf{I}_i \boldsymbol{\omega}_i + \mathbf{R}_o^i \mathbf{I}_i \dot{\boldsymbol{\omega}}_i + \mathbf{c}_o^i \times m_i \ddot{\mathbf{c}}_o^i) \tag{12}$$

A reference point with position vector $\mathbf{b}_o$ is now introduced that is chosen to lie on a tipover axis. The quantity $\tilde{\mathbf{M}}_b$ is computed with respect to this point, as:

$$\tilde{\mathbf{M}}_b \equiv \sum_{i=1}^{l} \mathbf{b}_o \times \mathbf{F}_o^i + \sum_{i=1}^{l+1} \mathbf{b}_o \times m_i \mathbf{g}_o + \sum_{i=1}^{k} \mathbf{b}_o \times \mathbf{B}_o^i \tag{13}$$

As stated above, $\mathbf{M}_o$ is the sum of moments with respect to a point fixed in an inertial frame. Taking the difference $\mathbf{M}_o - \tilde{\mathbf{M}}_b$ yields an expression for the sum of moments with respect to arbitrary point $\mathbf{b}_o$. This is illustrated in Figure 6 and computed as:

$$\mathbf{M}_o - \tilde{\mathbf{M}}_b = \sum_{i=1}^{l} (\mathbf{p}_o^i - \mathbf{b}_o) \times \mathbf{F}_o^i + \sum_{i=1}^{l+1} (\mathbf{c}_o^i - \mathbf{b}_o) \times m_i \mathbf{g}_o + \sum_{i=1}^{k} (\mathbf{q}_o^i - \mathbf{b}_o) \times \mathbf{B}_o^i \tag{14}$$

Next, Equation (14) is expressed in a body-fixed frame at $\mathbf{b}_o$ with the following simplifying definitions: $\mathbf{p}_b^i \equiv \mathbf{R}_b^o(\mathbf{p}_o^i - \mathbf{b}_o)$, $\mathbf{c}_b^i \equiv R_b^o(\mathbf{c}_o^i - \mathbf{b}_o)$, $\mathbf{q}_b^i \equiv \mathbf{R}_b^o(\mathbf{q}_o^i - \mathbf{b}_o)$, $\mathbf{F}_b^i \equiv \mathbf{R}_b^o \mathbf{F}_o^i$, and $\mathbf{B}_b^i \equiv \mathbf{R}_b^o \mathbf{B}_o^i$.

$$\mathbf{R}_b^o(\mathbf{M}_o - \tilde{\mathbf{M}}_b) = \sum_{i=1}^{l} \mathbf{p}_b^i \times \mathbf{F}_b^i + \sum_{i=1}^{l+1} \mathbf{c}_b^i \times m_i \mathbf{R}_b^o \mathbf{g}_o + \sum_{i=1}^{k} \mathbf{q}_b^i \times \mathbf{B}_b^i \tag{15}$$

Then using Equation (9):

$$\mathbf{R}_b^o(\mathbf{M}_o - \tilde{\mathbf{M}}_b) = \mathbf{R}_b^o(\dot{\mathbf{H}}_o - \tilde{\mathbf{M}}_b) \tag{16}$$

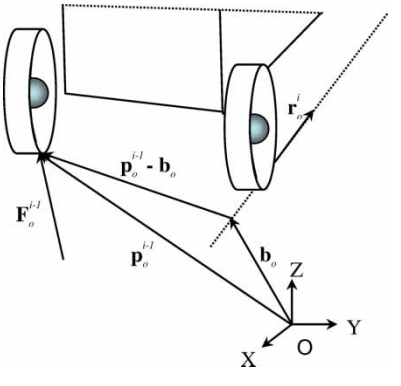

Figure 6. Illustration of force moment arms.

Prior to substituting $\tilde{\mathbf{M}}_b$ into (16), $\tilde{\mathbf{M}}_b$ is simplified, first grouping terms:

$$\tilde{\mathbf{M}}_b = \mathbf{b}_o \times \left[\sum_{i=1}^{l} \mathbf{F}_o^i + \sum_{i=1}^{l+1} m_i \mathbf{g}_o + \sum_{i=1}^{k} \mathbf{B}_o^i \right] \tag{17}$$

then using Newton's second law:

$$\sum_{i=1}^{l} \mathbf{F}_o^i + \sum_{i=1}^{l+1} m_i \mathbf{g}_o + \sum_{i=1}^{k} \mathbf{B}_o^i = \sum_{i=1}^{l+1} m_i \ddot{\mathbf{c}}_o^i \tag{18}$$

The term $\mathbf{R}_b^o(\dot{\mathbf{H}}_o - \tilde{\mathbf{M}}_b)$ is conveniently expressed using the previous definition $\mathbf{c}_b^i \equiv \mathbf{R}_b^o(\mathbf{c}_o^i - \mathbf{b}_o)$ as:

$$\mathbf{R}_b^o(\dot{\mathbf{H}}_o - \tilde{\mathbf{M}}_b) = \sum_{i=1}^{l+1} \mathbf{R}_b^i(\boldsymbol{\omega}_i \times \mathbf{I}_i \boldsymbol{\omega}_i + \mathbf{I}_i \dot{\boldsymbol{\omega}}_i) + \sum_{i=1}^{l+1} \mathbf{c}_b^i \times m_i \mathbf{R}_b^o \ddot{\mathbf{c}}_o^i \tag{19}$$

The modified conservation equation (16) is now restated, using Equations(15) and (19), as:

$$\begin{aligned} &\sum_{i=1}^{l} \mathbf{p}_b^i \times \mathbf{F}_b^i + \sum_{i=1}^{l+1} \mathbf{c}_b^i \times m_i \mathbf{R}_b^o \mathbf{g}_o + \sum_{i=1}^{k} \mathbf{q}_b^i \times \mathbf{B}_b^i \\ &\quad = \sum_{i=1}^{l+1} \mathbf{R}_b^i(\boldsymbol{\omega}_i \times \mathbf{I}_i \boldsymbol{\omega}_i + \mathbf{I}_i \dot{\boldsymbol{\omega}}_i) + \sum_{i=1}^{l+1} \mathbf{c}_b^i \times m_i \mathbf{R}_b^o \ddot{\mathbf{c}}_o^i \end{aligned} \tag{20}$$

Finally, an expression for the sum of moments caused by contact forces is given as:

$$\sum_{i=1}^{l} \mathbf{p}_b^i \times \mathbf{F}_b^i = \sum_{i=1}^{l+1} \mathbf{R}_b^i(\boldsymbol{\omega}_i \times \mathbf{I}_i \boldsymbol{\omega}_i + \mathbf{I}_i \dot{\boldsymbol{\omega}}_i) + \sum_{i=1}^{l+1} \mathbf{c}_b^i \times m_i \mathbf{a}_b^i - \sum_{i=1}^{k} \mathbf{q}_b^i \times \mathbf{B}_b^i \tag{21}$$

with the definition of a c.g. fixed accelerometer output given by $\mathbf{a}_b^i \equiv \mathbf{R}_b^o(\ddot{\mathbf{c}}_o^i - \mathbf{g}_o)$.

Taking the dot product of Equation (21) with the jth tipover axis $\mathbf{r}_b^j$ leads to:

$$\left[\sum_{i=1}^{l} \mathbf{p}_b^i \times \mathbf{F}_b^i \right] \cdot \mathbf{r}_b^j = \left[\sum_{i=1}^{l+1} \mathbf{R}_b^i(\boldsymbol{\omega}_i \times \mathbf{I}_i \boldsymbol{\omega}_i + \mathbf{I}_i \dot{\boldsymbol{\omega}}_i) + \sum_{i=1}^{l+1} \mathbf{c}_b^i \times m_i \mathbf{a}_b^i - \sum_{i=1}^{k} \mathbf{q}_b^i \times \mathbf{B}_b^i \right] \cdot \mathbf{r}_b^j \tag{22}$$

The left side of Equation (22) is equivalent to the direct SM defined in Equation (5). Thus the right side of Equation (22) is the indirect SM. Any known disturbance forces can be included in the computation. If no unknown disturbances are acting, the indirect SM is an equivalent expression of the SM that is composed of measurable inertial quantities.

3.3. *Analysis of sensing requirements*

The indirect SM requires knowledge or measurements of the following quantities:

(1) Angular velocity, angular acceleration, and linear acceleration of the vehicle chassis and wheels, expressed in a body-fixed frame.
(2) Knowledge of the c.g. position of the chassis and wheels relative to the wheel–terrain contact points. This implies that measurement of suspension displacement (and knowledge of suspension kinematics) may be required.

(3) Knowledge of the magnitude and direction of any non-negligible body forces **B**.

An analysis of the effect of partial or incomplete sensory knowledge on metric accuracy is presented in Section 4.3.

4. Simulation results

In this section simulation results are presented to validate the accuracy of the indirect expression of the SM given in Equation (22). In Section 4.1, the vehicle model and simulation environment are described. In Section 4.2, simulation results for the indirect SM (22) are compared with other existing stability metrics in both on-road and road departure scenarios. In Section 4.3, practical implementation considerations for the indirect SM are analysed.

4.1. *Description of simulation environment*

A model of a generic high-centred light truck was developed in the commercial multibody dynamic simulation software package ADAMS. The vehicle features a double wishbone suspension, rack and pinion steering, and a V8 engine. The model is illustrated in Figure 7. Critical vehicle parameters are listed in Table 1.

Simulations of aggressive manoeuvres were conducted at a range of speeds in both on-road and off-road scenarios. For on-road scenarios, a flat road surface was modelled, and for off-road scenarios a flat road surface with sloped shoulders was modelled. A cross-section of the road departure terrain can be seen in Figure 8.

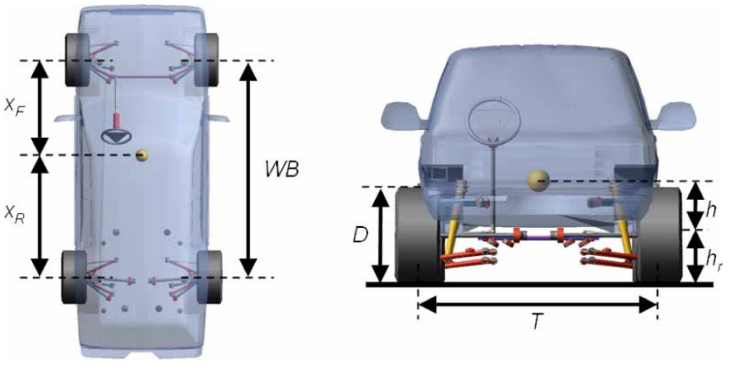

Figure 7. ADAMS vehicle model, plan and rear views.

Table 1. ADAMS model parameters.

Parameter	Value
Wheel base (WB)	2.56 m
Track width (T)	1.56 m
Wheel diameter (D)	0.70 m
Total mass (m)	2030 kg
Unsprung mass (m_{us})	150 kg
Body c.g. height (h)	0.34 m
Roll centre height (h_r)	0.37 m
Overall c.g. height ($h + h_r$)	0.71 m
Critical roll angle (φ_{cr})	10 deg
Critical acceleration (a_{cr})	1.25 g

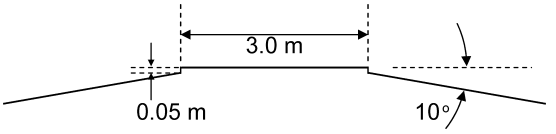

Figure 8. Road cross-section for road departure scenario.

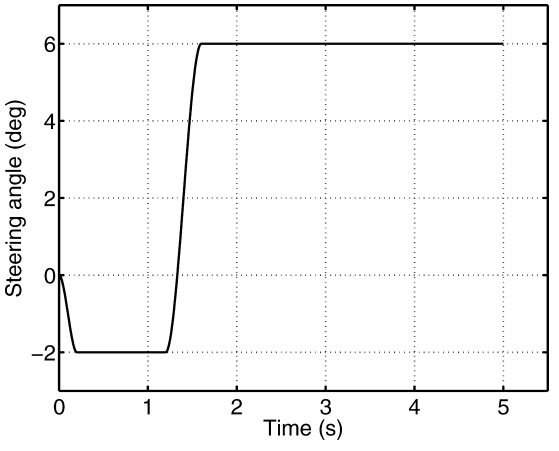

Figure 9. Fishhook steering input.

Both on-road and off-road terrains were modelled as rigid surfaces. To ensure that rollover (rather than skidding) was induced during simulated manoeuvres, an artificially large friction coefficient of 2.0 was used on all terrain surfaces.

The aggressive manoeuvre chosen for these tests was the fishhook manoeuvre, a manoeuvre employed in a standard governmental rollover tests. The manoeuvre consists of an open-loop steering input shown in Figure 9, performed at a near-constant vehicle speed (i.e. with no throttle or braking input). The steering input involves a step steer in one direction followed by a large counter steer in the opposite direction, which causes substantial excitation of vehicle roll dynamics.

Simulations were conducted at 9, 18, 27, 36, and 45 m/s (20, 40, 60, 80, and 100 mph) on each terrain surface. Illustrations of representative vehicle trajectories undergoing a fishhook manoeuvre in both on-road and off-road conditions are shown in Figures 10 and 11.

It was observed that, for on-road scenarios, wheel lift-off and vehicle rollover occurred at speeds of 27, 36, and 45 m/s. For off-road scenarios, wheel lift-off and vehicle rollover occurred at speeds of 18, 27, 36, and 45 m/s.

4.2. *Comparison vehicle of stability measurement metric accuracy*

The accuracy of the indirect SM metric of Equation (22) was compared to three other existing methods for each simulated trial. The ground truth of vehicle stability was taken as the load transfer of Equation (1), computed with the true wheel–terrain normal forces are available in simulation.

The first existing metric is the critical lateral acceleration, which assumes that wheel lift-off occurs when the lateral acceleration of the body exceeds a threshold acceleration a_{cr} (Table 1). The critical lateral acceleration is computed as:

$$R_{ay} = \frac{a_y}{a_{cr}} \tag{23}$$

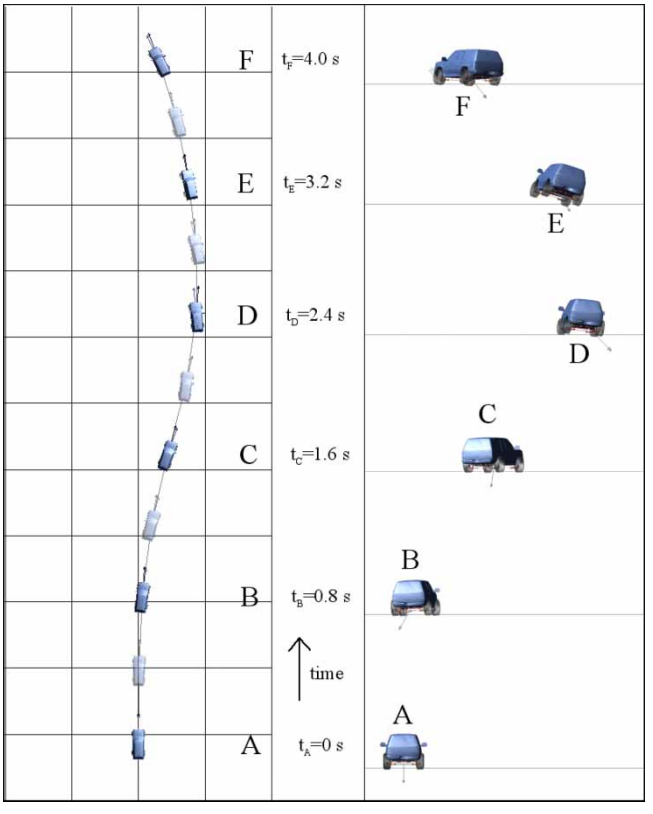

Figure 10. Vehicle trajectory for on-road fishhook at 27 m/s.

The second existing metric is the critical roll angle, which assumes that wheel lift-off occurs when the body roll angle exceeds a threshold roll angle φ_{cr} (Table 1). The critical roll angle is computed as:

$$R_{\text{roll}} = \frac{\varphi}{\varphi_{\text{cr}}} \tag{24}$$

The third existing metric is here termed the Odenthal estimate, named for the lead author of [6] in which it was proposed. The method is based on a linear suspension roll model where h_{r} is the roll centre height and h is the body c.g. height above the roll centre. The method incorporates lateral acceleration and roll angle and is computed as:

$$R_{\text{Oden}} = \frac{2m_{us}}{mT}\left[(h_r + h\cos\varphi)\frac{a_y}{g} + h\sin\varphi\right] \tag{25}$$

To quantify performance over all simulation trials, a number of performance measures are considered. The root mean square (RMS) and maximum values of error for each measure are computed as:

$$\text{RMS} = \sqrt{\frac{\sum_{i=1}^{N}(R_i - R)^2}{N}} \tag{26}$$

$$\text{MAX} = \arg\max(R_i - R) \tag{27}$$

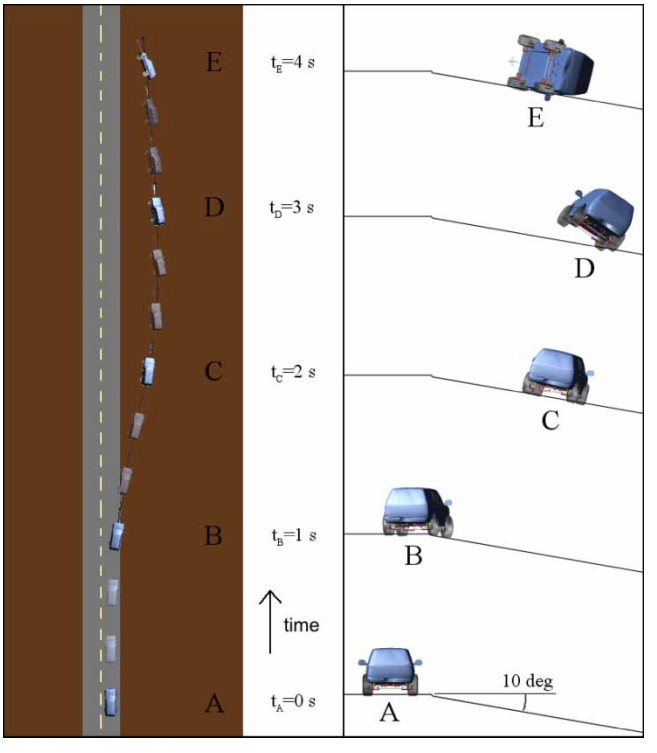

Figure 11. Vehicle trajectory for off-road fishhook at 27 m/s.

where N is the total number of trials. A third performance measure describes wheel lift-off detection accuracy as the fraction of lift-off time correctly identified by the detector. According to the definition of R in Equation (1), wheel lift-off occurs when $R = \pm 1$. To reduce chattering of wheel lift-off detectors in the presence of noisy signals, lift-off is deemed to begin when the absolute value of a load transfer metric exceeds a threshold of 0.95. The ground truth for wheel lift-off detection is taken from the response of a wheel lift-off detector to the ground truth load transfer metric. A fourth performance measure describes the metric false positive measure as the fraction of non-lift-off time incorrectly identified as lift-off. Finally, a fifth performance measure describes lift-off detection lag as the time difference between the beginning of wheel lift-off for the measure of interest and the ground truth.

Simulation results for an on-road fishhook manoeuvre at 27 m/s are shown in Figure 12a–d. The SM and the three alternative metrics are compared with the ground truth metric. No wheel lift-off was observed in this trial. It can be seen that each stability metric closely matches the ground truth.

Simulation results for a fishhook manoeuvre during road departure at 27 m/s are shown in Figure 13a–d. In these simulations, the vehicle departed the road from $t = 1.0$–1.8 s and re-entered at $t = 3.00$ s, at which time it was very near wheel lift-off. A small impulse from the road edge transition caused the vehicle to lift-off at $t = 3.00$ s, though it returned to full ground contact at $t = 3.75$ s.

It can be observed that, as in the on-road scenario, the indirect SM tracks the true load transfer with small deviation before, during, and after wheel lift-off. The Odenthal and critical lateral acceleration metrics shown in Figure 13b and d, respectively, are approximately correct until $t = 2.3$ s, when both underestimate the load transfer and erroneously indicate vehicle safety during wheel lift-off. The critical roll angle metric shown in Figure 13d deviates substantially

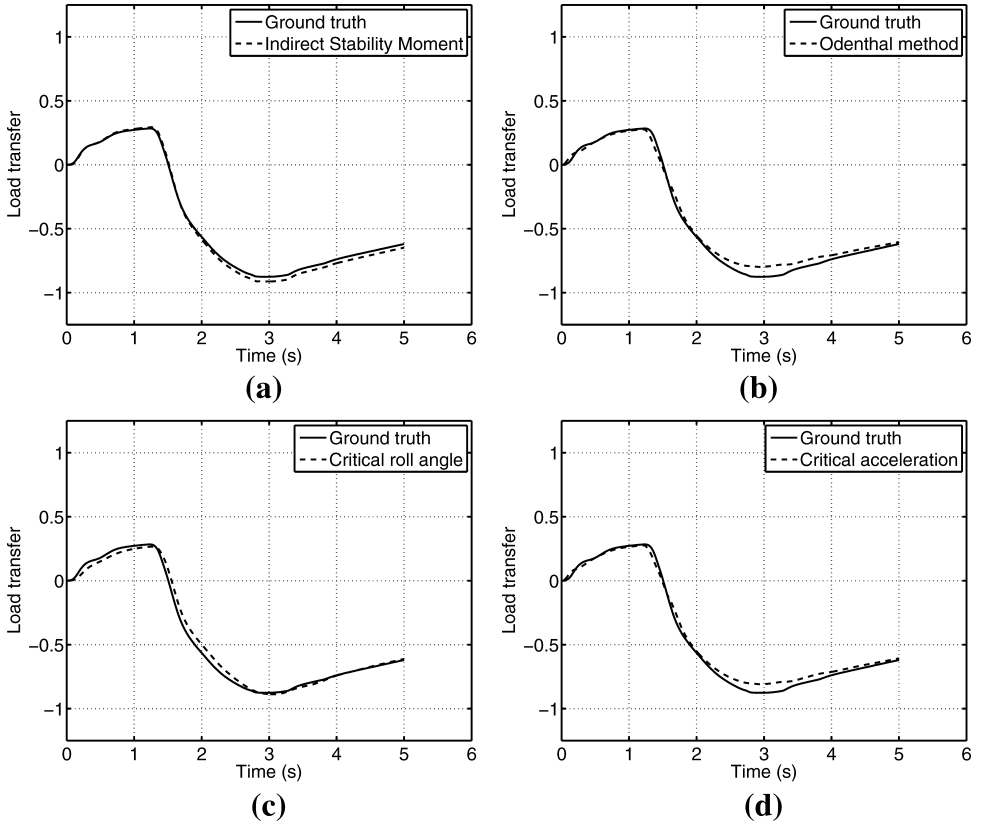

Figure 12. On-road stability metric performance comparison: (a) indirect SM, (b) Odenthal method, (c) critical roll angle, (d) critical lateral acceleration.

as soon as the vehicle departs the road surface, and incorrectly indicates wheel lift-off for the duration of off-road travel. These inaccuracies are caused by ignorance of the vertical mass acceleration, angular acceleration of the roll inertia, and changes in suspension configuration, all of which are considered in the indirect SM metric.

Average values for the five performance measures are shown in Figure 14a–e for the on-road trials, off-road trials, and an average of all trials (i.e. at 18, 27, 36, and 45 m/s). In summary, the critical roll angle measure tends to underestimate vehicle stability, and exhibit a substantial number of false positives for wheel lift-off detection, with significant error. The critical lateral acceleration and Odenthal metric tend to overestimate vehicle stability and exhibit poor lift-off detection. The SM exhibits excellent vehicle stability prediction accuracy, with few false positives and small lift-off detection error.

These simulation results suggest that the indirect SM is an accurate measure of vehicle load transfer and wheel lift-off, and performs better than existing techniques, particularly in road-departure situations.

4.3. *Analysis of the effect of sensor availability and vehicle parameter uncertainty on SM metric performance*

The above analysis has assumed that all sensor quantities and vehicle parameters required for calculation of the SM metric are known. In practice, some sensor quantities may be unavailable,

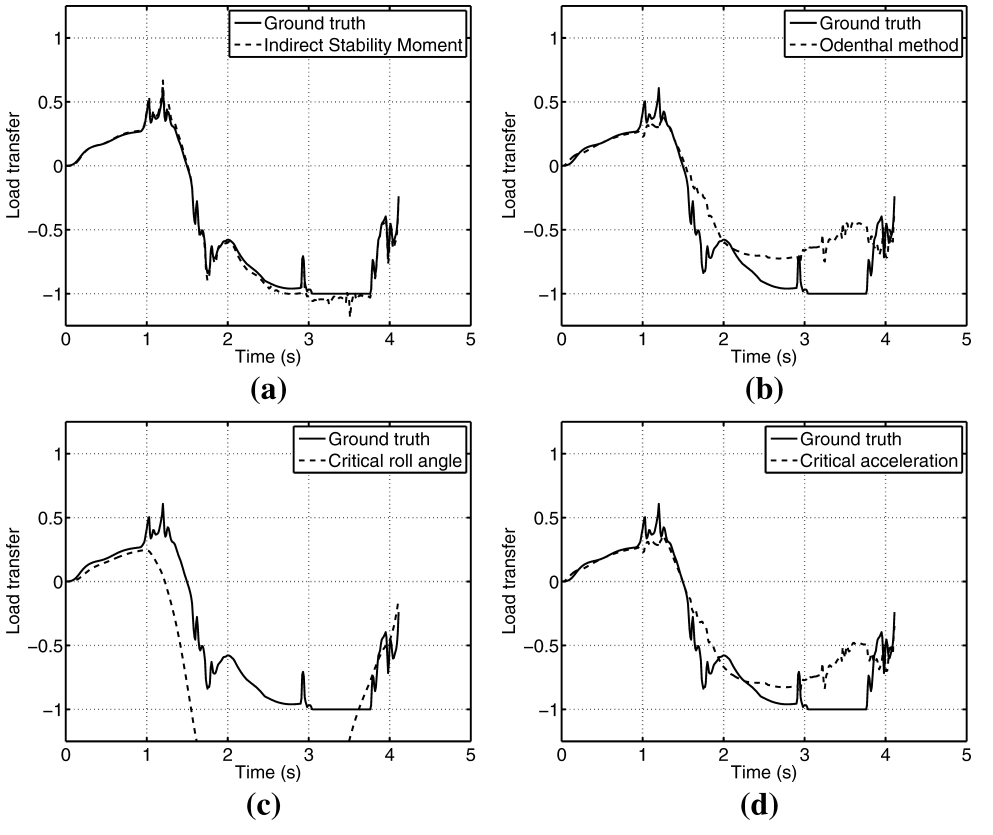

Figure 13. Off-road stability metric performance comparison: (a) indirect SM, (b) Odenthal method, (c) critical roll angle, (d) critical lateral acceleration.

and some vehicle parameters may be poorly known. The performance degradation of the SM with reduced sensor sets and parameter uncertainty is analysed in this section.

Four sensor sets, termed A–D, are defined with progressive reduction in available sensory information. The number of sensor axes used to measure body acceleration, body angular rate, suspension displacement, and wheel acceleration for each sensor set is summarised in Table 2. For this analysis, it is assumed angular acceleration is derived from angular rate and that no disturbances act on the vehicle.

Sensor set A is the most comprehensive, with three axes of sensing for body acceleration and angular rates as well as one axis of sensing for suspension displacement and vertical acceleration at each wheel. The SM for sensor set A is then:

$$\mathrm{SM}_j^A = \left[\mathbf{R}_b^{l+1}(\boldsymbol{\omega}_{l+1} \times \mathbf{I}_{l+1}\boldsymbol{\omega}_{l+1} + \mathbf{I}_{l+1}\dot{\boldsymbol{\omega}}_{l+1}) + \sum_{i=1}^{l+1} \mathbf{c}_b^i \times m_i \mathbf{a}_b^i \right] \cdot \mathbf{r}_b^j \tag{28}$$

Sensor set B is equivalent to suite A with the omission of wheel acceleration sensors. To account for the lack of wheel acceleration sensors, an estimate of the wheel acceleration based on rigid body kinematics is used:

$$\hat{\mathbf{a}}_b^i = \mathbf{a}_b^{l+1} + \mathbf{R}_b^i(\dot{\boldsymbol{\omega}}_{l+1} \times (\mathbf{c}_b^i - \mathbf{c}_b^{l+1}) + \boldsymbol{\omega}_i \times (\boldsymbol{\omega}_i \times (\mathbf{c}_b^i - \mathbf{c}_b^{l+1}))) \tag{29}$$

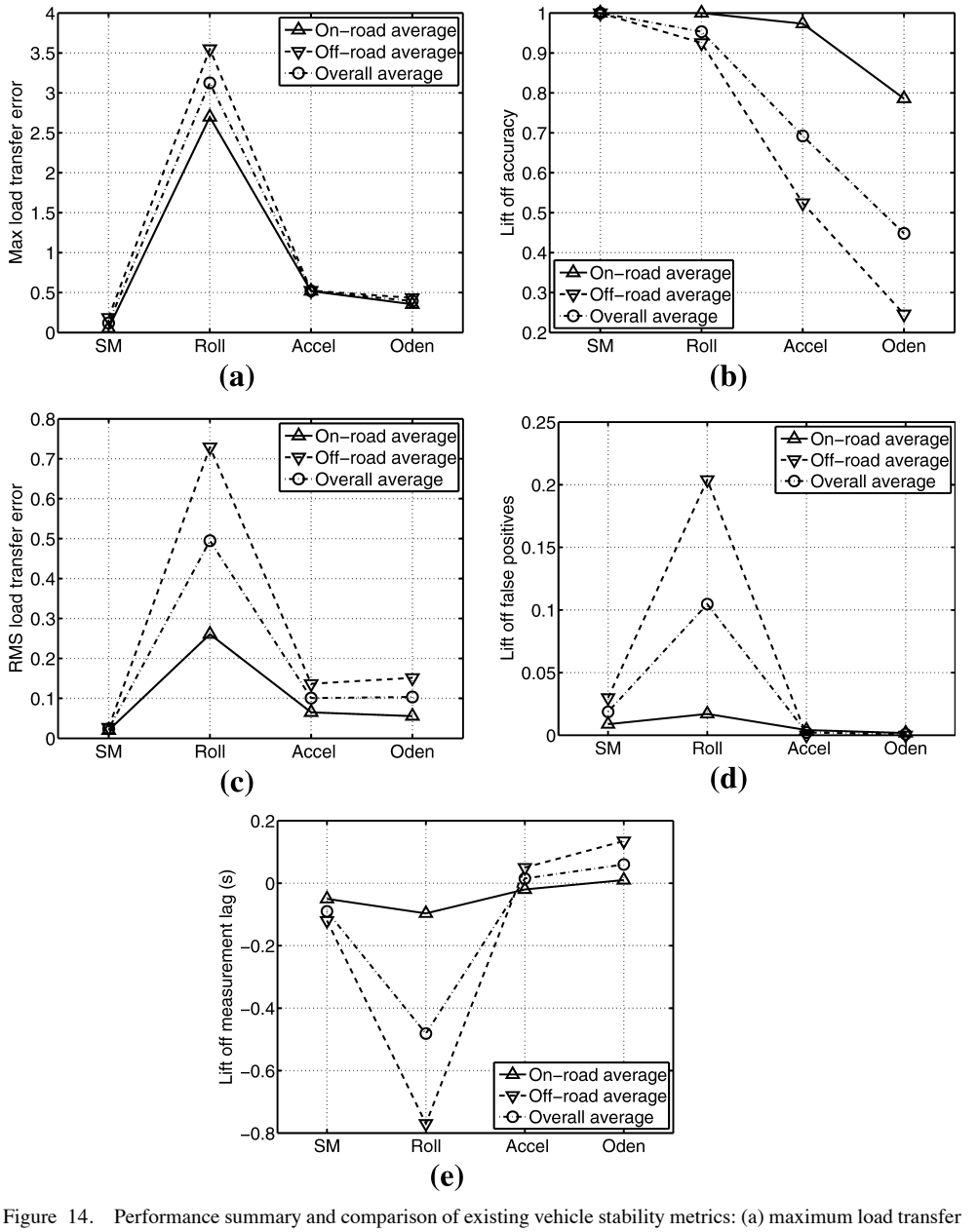

Figure 14. Performance summary and comparison of existing vehicle stability metrics: (a) maximum load transfer error, (b) lift-off accuracy, (c) RMS load transfer error, (d) lift-off false positives, (e) lift-off measurement lag.

Table 2. Number of sensor axes in reduced sensor sets.

Sensor set	Body acceleration	Body angular rate	Suspension displacement	Wheel vertical acceleration
A	3	3	4	4
B	3	3	4	
C	2	1		
D	2			

and the corresponding SM is:

$$\mathrm{SM}j^B = \left[\mathbf{R}_b^{l+1}(\boldsymbol{\omega}_{l+1} \times \mathbf{I}_{l+1}\boldsymbol{\omega}_{l+1} + \mathbf{I}_{l+1}\dot{\boldsymbol{\omega}}_{l+1}) + \sum_{i=1}^{l+1} \mathbf{c}_b^i \times m_i \hat{\mathbf{a}}_b^i\right] \cdot \mathbf{r}_b^j \tag{30}$$

Sensor set C omits suspension displacement sensors, so that position vectors $\mathbf{c}_b^i$ and tipover axes $\mathbf{r}_b^j$ are approximated with constant vectors $\hat{\mathbf{c}}_b^i$ and $\hat{\mathbf{r}}_b^j$. The approximate position vectors used in this study correspond to a 50% compression of each suspension member beyond static equilibrium compression. Assuming the approximate tipover axes $\hat{\mathbf{r}}_b^j$ are aligned with

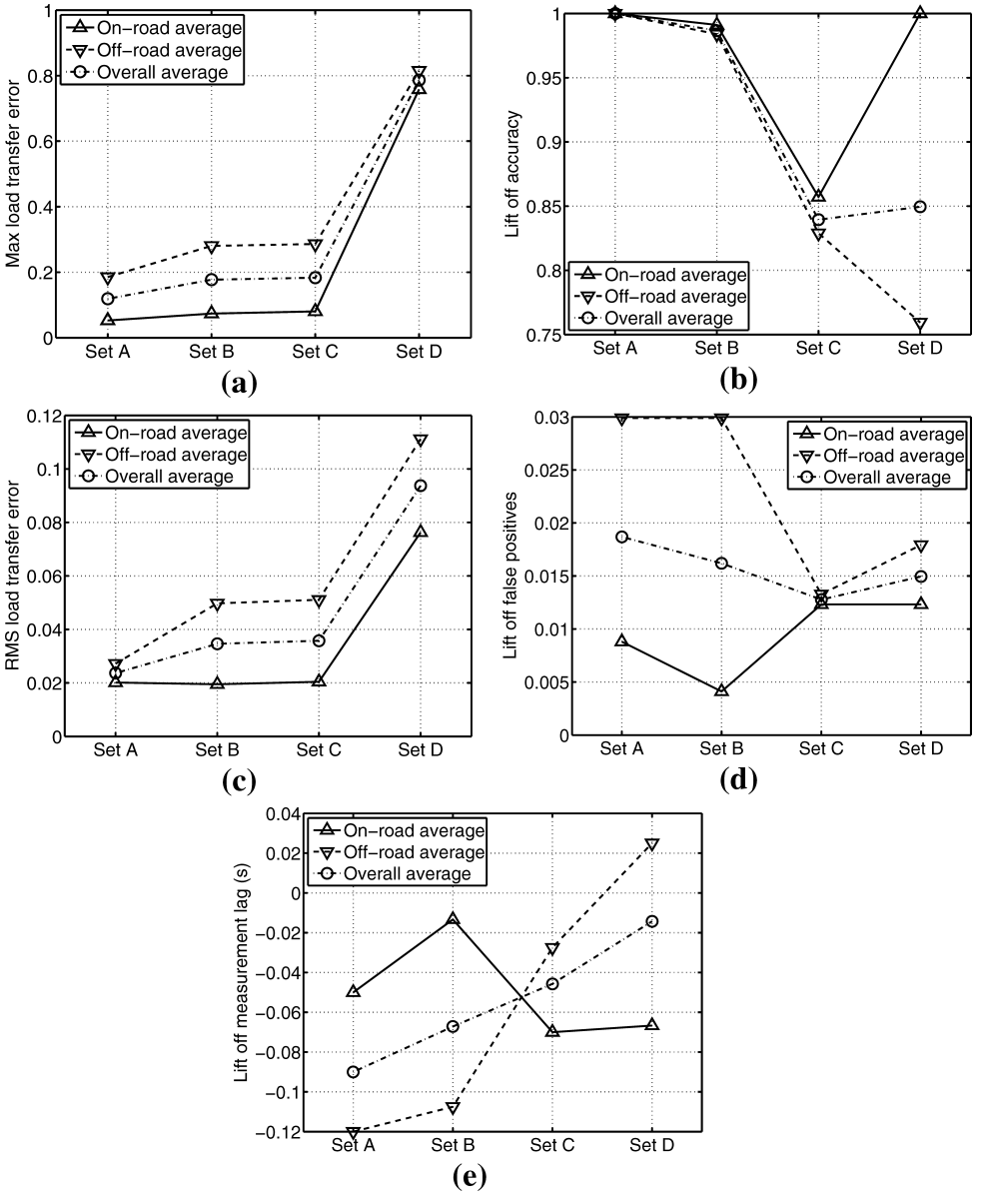

Figure 15. Sensor set performance comparison: (a) maximum load transfer error, (b) lift-off accuracy, (c) RMS load transfer error, (d) lift-off false positives, (e) lift-off measurement lag.

the vehicle roll axis, several terms can be eliminated from the SM computation. As such, body sensors for pitch and yaw angular rates and longitudinal acceleration are omitted as well. The SM for sensor set C is then:

$$\mathrm{SM}_j^C = \left[\mathbf{R}_b^{l+1}(\mathbf{I}_{l+1}\dot{\boldsymbol{\omega}}_{l+1}) + \sum_{i=1}^{L+1} \hat{\mathbf{c}}_b^i \times m_i \hat{\mathbf{a}}_b^i \right] \cdot \hat{\mathbf{r}}_b^j \tag{31}$$

which can be simplified to the following when $\hat{\mathbf{r}}_b^j = [1 \quad 0 \quad 0]^{\mathrm{T}}$, $\mathbf{R}_b^{l+1}$ is the identity matrix, and other terms are x, y, and z components of the corresponding vectors:

$$\mathrm{SM}_j^C = I_{xx}\dot{\boldsymbol{\omega}}_x + \sum_{i=1}^{l+1} m_i(\hat{c}_{by}^i \hat{a}_{bz}^i - \hat{c}_{bz}^i \hat{a}_{by}^i) \tag{32}$$

Finally, sensor set D omits the body roll rate sensor, so that it only utilises body lateral and vertical acceleration. Without any measurement of angular rates, the approximate wheel accelerations $\hat{\mathbf{a}}_b^i$ cannot be computed. As such, the measured body acceleration $\mathbf{a}_b^{l+1}$ alone is used to approximate each wheel acceleration. Under the conditions provided for computing Equation (32), the SM for sensor set D is:

$$\mathrm{SM}_j^D = \sum_{i=1}^{l+1} m_i(\hat{c}_{by}^i a_{bz}^{l+1} - \hat{c}_{bz}^i a_{by}^{l+1}) \tag{33}$$

The performance of the SM metric was analysed in simulation for fishhook manoeuvres in both on-road and road departure scenarios, assuming the availability of sensor suites A–D. These results are shown in Figure 15a–e. It can be observed that reducing the number of available sensors tends to increase metric error, with the largest increase in error observed between sensor suites C to D. This indicates that vehicle body angular acceleration is critical to accurate measurement of stability. Wheel lift-off accuracy also decreases as the number of available sensors decreases, with the loss of suspension displacement sensors here causing the largest decrease. In general, it can be observed that SM metric performance degrades relatively gracefully with reduced sensor availability.

5. Experimental results

In this section, the performance of the SM metric is analysed in a series of experimental trials. Three high-speed aggressive manoeuvres were conducted on flat ground with an experimental vehicle instrumented with sensors to measure linear vehicle body acceleration (i.e. a three-axis accelerometer), vehicle body angular rates (i.e. a three-axis rate gyroscope), and suspension displacement (i.e. independent suspension potentiometers). This allows analysis of metric performance with sensor sets B, C, and D of Section 4.3. The experimental vehicle was a light truck with parameters similar to those given in Table 1.

Since a direct measure of wheel–terrain contact forces was unavailable for these experiments, the absolute load transfer error could not be evaluated. Instead, ground truth for wheel lift-off was determined by observing when the suspension displacement sensor reached its hard stop. This corresponds to full extension of the spring and thus strongly suggests that the wheel had lifted off. This enabled evaluation of the three lift-off performance metrics.

The experimental manoeuvre was a double lane change, executed with an initial speed of 47 m/h. The vehicle trajectory for the first experimental trial (as measured by GPS) is shown

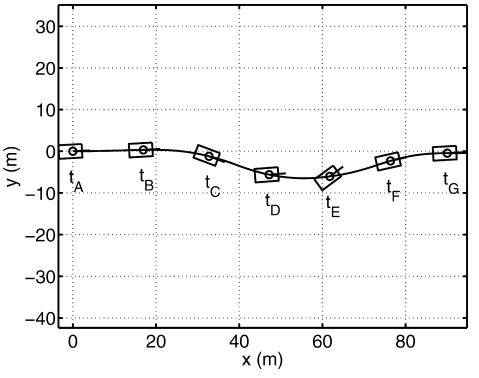

Figure 16. Double lane change path.

in Figure 16. Points of interest are labelled A–G. Vehicle speed remained relatively constant during the manoeuvre, since the throttle was not applied after time $t_B \approx 0.7$ s, and brakes were not applied at all during the manoeuvre.

Wheel lift-off occurred in the first trial between times $t_B = 0.71$ s and $t_C = 1.43$ s and immediately after time $t_D = 2.16$ s. These times corresponded to a large amplitude steering input from the vehicle and a resulting large body roll. The SM metric computed with sensor set B can be seen in Figure 17. It can be observed that the SM accurately indicated the two periods of wheel lift-off.

Quantitative results for all three trials are summarised in Table 3. It can be observed that the SM metric accurately predicted wheel lift-off with a small rate of false positives.

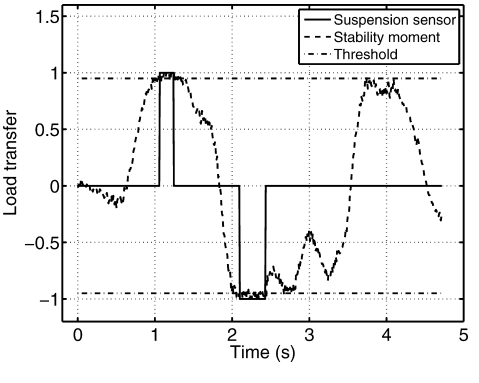

Figure 17. Load transfer and wheel lift-off.

Table 3. Experimental results.

Trial	1	2	3	Average
Lift-off accuracy (%)	93	97	100	97
False positives (%)	2.8	1.0	1.5	1.8

6. Discussion and conclusion

This paper has presented a novel vehicle stability metric, termed the SM. In Section 4, simulation results of aggressive manoeuvres on flat terrain and in road departure were presented that validate the metric's accuracy. Several metrics were introduced, based on load transfer estimation error and performance of a simple wheel lift-off detector. The estimation error quantifies the accuracy of the metric over the entire range of conditions, while the lift-off detector focuses on accuracy during particularly extreme conditions. In Figure 14a and c, the load transfer estimation error is shown to be smaller for the SM than existing methods for the considered scenarios, particularly during road departure. In Figure 14b and d, the SM is shown to have the best combination of high-lift-off identification accuracy and low false positive rate. Although the Odenthal and acceleration metrics have lower false positive rates, their lift-off accuracy is very poor during road departure. Lift-off detection accuracy and false positive rate can be independently improved by changing the threshold of each metric, but improvement in one will be balanced by degradation of the other.

Simulation results were also used to estimate the degradation in performance of the indirect SM with reduced sensory information. In Figure 15c, the loss of wheel accelerometers and suspension displacement sensors increased average RMS load transfer error from 0.024 to 0.038, while the loss of body roll rate sensing increased RMS load transfer error to 0.095. This indicates the relative importance of the roll rate sensor in comparison to suspension displacement and wheel acceleration for load transfer estimation. In Figure 15b, it can be seen that the loss of suspension displacement sensing causes a drop in lift-off detection accuracy from about 98% to 85%. For a given application, the sensing set should be chosen based on the relative importance of load transfer accuracy during all conditions and during lift-off conditions.

In Section 5, experimental results were presented for aggressive manoeuvres on flat terrain. Since a ground truth of load transfer was not available, the SM was validated through wheel lift-off detection, with an average accuracy of 97% and 1.8% false positive rate. These results correspond to the performance predicted in simulation for sensor set B. An opportunity for future work is to conduct experiments with a ground truth of load transfer using wheel force transducers on both flat terrain and in road departure. Additionally, the metric could be evaluated in more general off-road terrain, since its derivation provides for arbitrary terrain.

Rollover stability measurement in on-road and road departure conditions is important for the development of next-generation stability control systems. A topic of continuing study is the development of rollover stability control algorithms based on the SM, which may prove to be more robust in road departure scenarios.

References

[1] National Highway Traffic Safety Administration, *Traffic Safety Facts 2004: A Compilation of Motor Vehicle Crash Data from the FARS and the GES* (DOT HS 809 919), National Highway Traffic Safety Administration, Washington, DC, 2006.
[2] D. Blower, J. Woodrooffe, P. Green, A. Matteson, and M. Shrank, *Determination of events leading to sport utility vehicle rollovers*, Transport. Res. Record 1908 (2005), pp. 180–186.
[3] J. Viner, *Risk of rollover in ran-off-road crashes*, Transport. Res. Record 1500 (1995), pp. 112–118.
[4] DARPA Grand Challenge Web Site. Available at: www.darpa.mil/grandchallenge/
[5] B. Leedy, J. Putney, C. Bauman, S. Cacciola, J.M. Webster, and C.F. Reinholtz, *Virginia Tech's twin contenders: A comparative study of reactive and deliberative navigation*, J. Field Robot. 23(9) (2006), pp. 709–727.
[6] D. Odenthal, T. Bünte, and J. Ackerman, *Nonlinear steering and braking control for vehicle rollover avoidance*, Proceedings of European Control Conference, Karlsruhe, Germany, 1999.
[7] B. Chen and H. Peng, *Differential-braking-based rollover prevention for sport utility vehicles with human-in-the-loop evaluations*, Veh. Syst. Dyn. 36(4–5) (2001), pp. 359–389.

[8] C. Carlson and J.C. Gerdes, *Optimal rollover prevention with steer by wire and differential braking*, Proceedings of the ASME Dynamic Systems and Control Division – 2003, Washington, DC, pp. 345–354, 2003.
[9] P. Weissler, *Rollover safety in Volvo's XC90*, Auto. Eng. 110(10) (2002), pp. 12–13.
[10] R.B. McGhee and A.A. Frank, *On the stability properties of quadruped creeping gait*, Math. Biosci. 3(2) (1968), pp. 331–351.
[11] R.B. McGhee and G.I. Iswandhi, *Adaptive locomotion of a multilegged robot over rough terrain*, IEEE Trans. Syst. Man Cybernet. SMC-9(4) (1979), pp. 176–182.
[12] S. Sugano, Q. Huang, and I. Kato, *Stability criteria in controlling mobile robotic systems*, IEEE/RSJ International Workshop on Intelligent Robots and Systems, Yokohama, Japan, July 1993, pp. 832–838.
[13] J.K. Davidson and G. Schweitzer, *A mechanics-based computer algorithm for displaying the margin of static stability in four-legged vehicles*, Trans. ASME J. Mech. Design 112 (1990), pp. 480–487.
[14] J.P. Chrstos and D.A. Guenther, *The measurement of static rollover metrics*, SAE Transactions no. 920582, 1992.
[15] E. Papadopoulos and D. Rey, *The force-angle measure of tipover stability margin for mobile manipulators*, Veh. Syst. Dyn. 33(1) (2000), pp. 29–48.
[16] K. Iagnemma, A. Rzepniewski, S. Dubowsky, and P. Schenker, *Control of robotic vehicles with actively articulated suspensions in rough terrain*, Auton. Robots 14(1) (2003), pp. 5–16.
[17] A. Diaz-Calderon and A. Kelly, *On-line stability margin and attitude estimation for dynamic articulating mobile robots*, Int. J. Robot. Res. 24(10) (2005), pp. 845–866.
[18] S.C. Peters and K. Iagnemma, *An analysis of rollover stability measurement for high-speed mobile robots*, Proceedings of 2006 IEEE International Conference on Robotics and Automation, Orlando, FL, May 2006, pp. 3711–3716.
[19] D. Wettergreen and C. Thrope, *Gait generation for legged robots*, Proceedings IEEE/RSF International Conference on Intelligent Robots and Systems, Raleigh, NC, 1992, pp. 1413–1420.
[20] A.G. Nalecz, Z. Lu, and K. LD'Entremont, *An investigation into dynamic measures of vehicle rollover propensity*, SAE Transactions no. 930831, 1993.
[21] B. Johansson and M. Gäfvert, *Untripped SUV rollover detection and prevention*, Proceedings of 43rd IEEE Conference on Decision and Control, Atlantis, Paradise Island, Bahamas, December 2004, pp. 5461–5466.
[22] J. Hahn, R. Rajamani, and L. Alexander, *GPS-based real-time identification of tire-road friction coefficient*, IEEE Trans. Control Syst. Technol. 10(3) (2002), pp. 331–343.
[23] L.R. Ray, *Nonlinear state and tire force estimation for advanced vehicle control*, IEEE Transactions on Control Systems Technology, 3(1) (1995), pp. 117–122.
[24] P.M. Siegrist and P.R. Mcaree, *Tyre-force estimation by Kalman inverse filtering: applications to off-highway mining trucks*, Veh. Syst. Dyn. 44(12) (2006), pp. 921–937.
[25] J. Bernard, J. Shannan, and M. Vanderploeg, *Vehicle rollover on smooth surfaces*, SAE Transactions no. 891991, 1989.
[26] A. Hac, *Rollover stability index including effects of suspension design*, SAE Transactions no. 2002-01-0965, 2002.